
Intelligent Trading System: Multidimensional financial time series clustering based on self-organizing map

Pei Dehao^a, Luo Chao^{a,b*}

School of Information Science and Engineering, Shandong Normal University, Jinan 250014, China

Abstract:

Multidimensional time series clustering is an important problem in time series data analysis. This paper provides a new research idea for the behavioral analysis of financial markets, using the intrinsic correlation existing between transactions in the same segment of the financial market to cluster and analyze multidimensional time-series data, so as to obtain different types of market characteristics. In this paper, we propose a multidimensional time series clustering model based on graph attention autoencoder (GATE) and mask self-organizing map (Mask-SOM), based on which we realize multi-step prediction of financial derivatives prices and intelligent trading system construction. To obtain and fully utilize the correlation features between multidimensional financial time series data containing high noise for clustering analysis, constant curvature Riemannian manifolds are introduced in the graph attention autoencoder, and the multidimensional financial time series features captured by the encoder are embedded into the manifold. Following that, the multidimensional financial time series clustering analysis is implemented using Mask-SOM analysis manifold encoding. Finally, the feasibility and effectiveness of the model are verified using real financial datasets.

1. Introduction

Time series clustering is a technique to classify a large amount of data without a prior knowledge, which can help researchers quickly comprehend the distribution pattern and spatial structure of data, and provide strong support for subsequent time series prediction, data mining or anomaly detection. The multidimensional financial time series contains the volatility characteristics of the financial market and hides the patterns of the financial market, so it is thus important to scientifically analyze multidimensional financial time series for avoiding market risks and guiding investments effectively. Compare with other time series, the characteristics of multidimensional financial time series such as high noise, strong volatility and

nonlinearity pose great challenges for achieving accurate clustering. How to reduce the influence of these features and achieve accurate and effective multidimensional financial time series clustering has become a research hotspot across multiple disciplines.

The self-organizing map (SOM)[1], also known as Kohonen network, was proposed by Professor Kohonen T in Finland. As a class of unsupervised learning models, SOM can automatically search the intrinsic patterns and essential attributes in samples, and self-organize and adaptively change the network parameters and structure to achieve clustering and feature learning of data. With its robust self-organized learning process, time series learning models based on the SOM model are widely proposed. For example, Hsu et al[2] introduced SOM to decompose a dataset containing heterogeneous data into multiple homogeneous regions and applied Support Vector Regression (SVR) to forecast financial time series in order to deal with the characteristics of non-stationary financial time series; Sarlin et al[3] introduced fuzzy C-means in SOM to cope with the hard to classify features of financial time series data, etc[4][5].The features of SOM order-preserving mapping make it an excellent visualization tool[6], and Fu et al[7] also applied self-organizing mapping neural networks to pattern discovery of financial time series. However, all the above models are for single-dimensional financial time series clustering, and the effective implementation of multidimensional time series clustering with SOM is still an urgent issue to be explored.

The emergence of graph attention networks (GAT)[8] has provided a new perspective for multidimensional time series analysis. In recent years, GAT performs feature extraction and sequence learning from multidimensional time series input data in an unsupervised approach. Many researchers structure multidimensional time series as graph structures and learn correlations among nodes, such as Zhao et al[9] who treat each univariate time series as a separate feature and use two parallel GAT layers to learn complex dependencies of multivariate time series in time and feature dimensions, respectively; Cheng et al[10] propose an attribute-driven graph attention network (AD-GAT) for learning correlations among listed companies, etc. In order to analyze the correlation between data and to generate deep high-level features, models based on graph neural networks[8][11] and encoder-decoder frameworks[12][13][14] have been proposed sequentially. Kosaraju et al[15] proposed a recurrent encoder-decoder architecture where GAT acts as an encoder responsible for encoding social interaction behaviors among humans and the trained model can predict human paths based on features. Grattarola et al[16] identified non-Euclidean spaces as more suitable for representing graph data than Euclidean spaces, and used graph convolutional

networks(GCN) and encoder-decoder framework to learn embeddings of graph structure data on constant-curvature Riemannian manifolds(CCMs). However, strong nonlinearity in the original financial data affects the validity of series encoding

For unsupervised clustering of large amounts of data, the K-means algorithm[17][18][19] is the most commonly used clustering algorithm due to its advantage of high computational efficiency. However, the clustering results of the K-means algorithm are unstable and the initial value has a great influence on the results of clustering convergence, in contrast, SOM can achieve more stable clustering results and is less affected by the initial value due to its introduction of a neighborhood function with topological structure, and many researchers have used SOM and its variants[20][21] for clustering financial time series. However, majority of the current mainstream unsupervised clustering methods[22] are using the Euclidean distance measure of similarity in the Euclidean space, and the problem of high global similarity caused by small variance features in the input vector, which seriously affects the effect of volatility analysis and prevents the refinement of clustering. Niennattrakul et al[23]demonstrated that neither the K-means algorithm based on Euclidean distance nor Dynamic Time Warping (DTW) as a distance metric can correctly accomplish shape similarity clustering. Liu et al[24] demonstrated the drawbacks of using Euclidean distance for shape similarity measures. Therefore, it is of significance to optimize the distance metric function and try to analyze financial time series data in non-Euclidean space.

The manifold is a space with the characteristics of a local Euclidean space. Zhou et al[25] proposed that although the data samples one observes or collects are high-dimensional, what is closely related to the learning task may only be a certain low-dimensional distribution, i.e., a low-dimensional embedding in a high-dimensional space. Tenenbaum et al[26] proposed that it is misleading to compute straight-line distances directly in a high-dimensional space after the low-dimensional manifold is embedded into the high-dimensional space. To analyze the stream shape distribution of data, some stream shape learning[27][28], stream shape clustering[29][30], and stream shape embedding clustering[31][32][33] methods have been gradually proposed since 2000. Some researchers started to try to analyze financial time series data in manifolds, for example, Han et al[34] introduced structured manifold learning methods in forecasting models and proposed a Structured Manifold Broad Learning system (SM-BLS) that can recover chaotic attractors from multivariate and heterogeneous time series; Feng et al[35] proposed a Robust Manifold Broad Learning System (RM-BLS) by mining the evolution patterns of chaotic time series using

stream embedding technique; Papaioannou et al[36] proposed a three-layer high-dimensional time series forecasting model based on a manifold learning framework, which first embeds the time series into a low-dimensional space, then constructs a reduced-order regression model on the manifold, and finally lifts the embedded time series back to the original high-dimensional space using radial basis functions and geometric harmonics, which enables financial time series forecasting.

Based on the above problems and existing works, we study a hybrid model for clustering and analyzing the overall fluctuation information of multidimensional time series. First, the model is based on encoder-decoder architecture and GAT, and introduces constant-curvature Riemannian manifolds into the model to realize the embedding learning of sequence data features in the manifold space, which reduces the interference of strong nonlinearity on the clustering of fluctuation information. Second, we propose a recursive clustering algorithm, Mask-SOM, to realize the clustering analysis of multidimensional financial time series features on the manifold space, and then, complete the prediction of multidimensional financial time series fluctuation directions. Our contributions are summarized as follows:

- 1) Unlike traditional financial time series forecasting, we use the intrinsic correlation that exists between transactions in the same segment of the financial market to perform multidimensional time-series data clustering analysis, thus obtaining different types of market characteristics and providing a new research idea for financial market behavior analysis.
- 2) In order to unsupervised learn the mutual correlation of multidimensional financial time series, we construct a model based on encoder-decoder architecture and GAT, and introduce constant curvature Riemannian manifolds into the model for the problem of strong nonlinearity of financial time series in Euclidean space to realize the learning of multidimensional financial time series features in manifolds.
- 3) In order to realize the clustering analysis of features in manifolds and improve the weaknesses of the Euclidean distance metric, we learned the idea of Principle Component Analysis (PCA) and innovatively proposed a novel SOM model, Mask-SOM, which learns the data distribution from coarse to fine granularity in an incremental manner to implement feature clustering and prediction of financial time series data with strong nonlinearity.

2. Manifold clustering model based on graph attention autoencoder

The manifold clustering model based on graph attention autoencoder consists of three main components. Firstly, in order to effectively characterize the sector volatility and circumvent the effect of high financial time series noise, the original financial time series data is no longer used as input to the model, but the price and volume volatility characteristics of the original financial time series data extracted from the sliding window. Secondly, to deal with the strong nonlinearity of financial time series in the Euclidean space, the constant curvature manifolds are introduced into the graph attention autoencoder and construct the graph attention manifold autoencoder(GATME) to accomplish the learning of time series features in the manifold. Finally, in order to complete the clustering analysis of features in the manifold, we innovatively propose Mask-SOM to achieve feature clustering of high-noise multidimensional financial time series data. The model structure is shown in Figure 1.

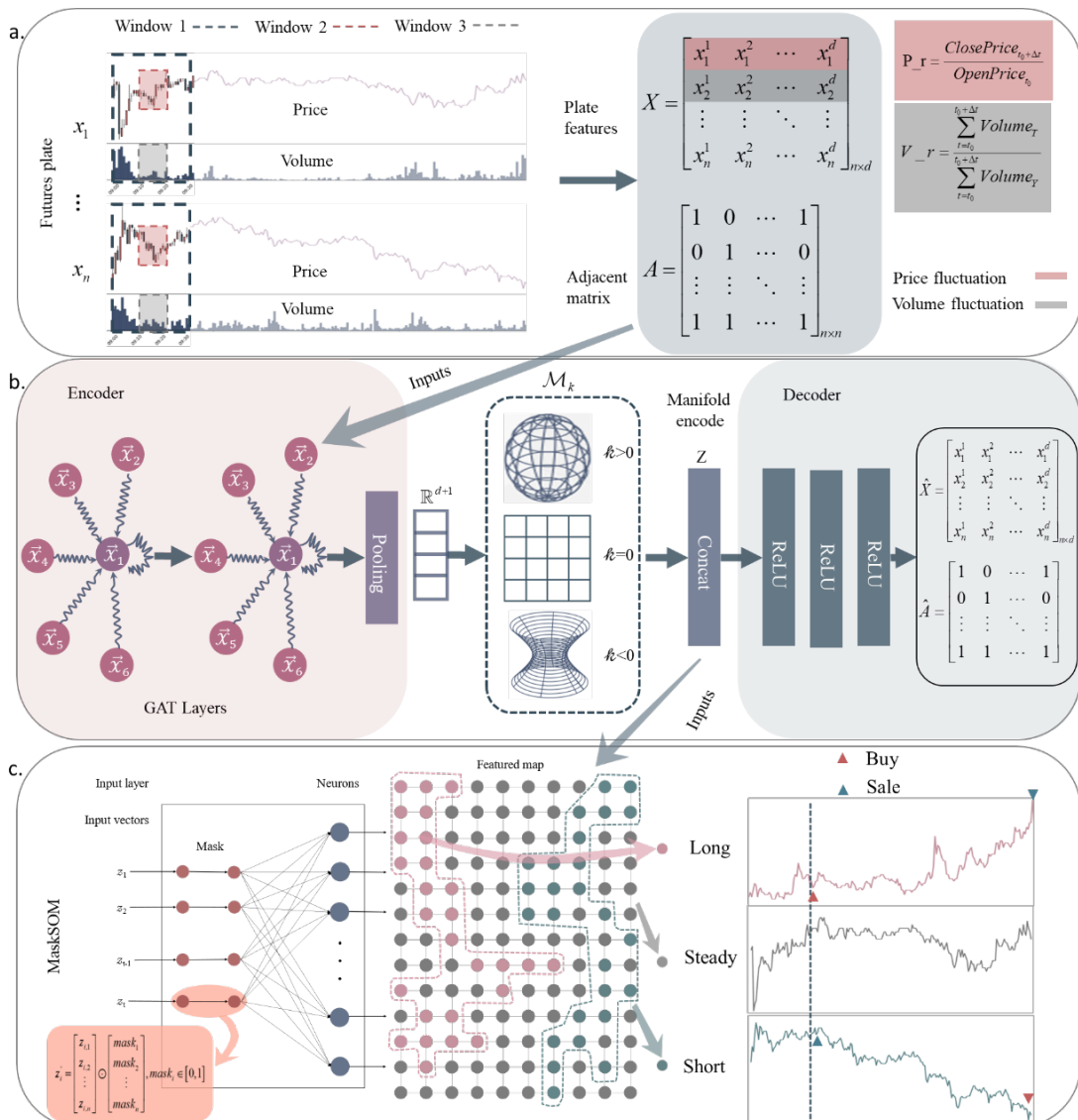


Figure 1 Manifold clustering model based on graph attention autoencoder

2.1 GATME

First, a sliding window is used to extract the features of n financial products in a financial segment. As shown in Figure 1.a, window 1 is a time window, sliding window 2 and sliding window 3 in window 1 are responsible to extract price fluctuation features and volume fluctuation features respectively, and integrating them into the segment features \mathbf{X} . After that, the extracted segment features \mathbf{X} and the predefined adjacency matrix \mathbf{A} are fed into the GATME. As shown in Figure 1.b, the encoder of GATME uses GAT, receives the input $[\mathbf{X}, \mathbf{A}]$ and learns the graph representation, and the decoder uses a fully connected neural network, reconstructs the latent representation and maps it to the graph space. The training goal is to minimize the reconfiguration loss of node features and the graph structure as follows:

$$Loss = \frac{1}{N} \sum_{i=1}^N \|X_i - \hat{X}_i\| - \frac{1}{N^2} \sum_{i,j} (A_{i,j} \log \hat{A}_{i,j} + (1 - A_{i,j}) \log(1 - \hat{A}_{i,j})) \quad (1)$$

The trained GATME will discard the decoder and keep only the encoder and manifold embedding parts.

The architecture of the GAT layer following the work of Velickovic et al[8]. The input to the GAT layers is a multidimensional time series feature \mathbf{X} :

$$\mathbf{X} = \{\vec{x}_1, \vec{x}_2, \dots, \vec{x}_N\}, \vec{x}_i \in R^F$$

Where N is the number of nodes, and F is the number of features in each node. The layer generates a new set of features with dimension F' :

$$\mathbf{X}' = \{\vec{x}'_1, \vec{x}'_2, \dots, \vec{x}'_N\}, \vec{x}'_i \in R^{F'}$$

In order to obtain sufficient expressive power to transform the input features into higher-level features, a shared linear transformation, parametrized by a weight matrix, $\mathbf{W} \in R^{F' \times F}$, is applied to every node. Then perform self-attention on the node—a shared attentional mechanism $a: R^{F'} \times R^{F'} \rightarrow$ computes attentions coefficients

$$e_{ij} = a(\mathbf{W}\vec{x}_i, \mathbf{W}\vec{x}_j) \quad (2)$$

that indicate the importance of node j 's feature to node i , $j \in N_i$, N_i denote the immediate neighbor of i . To make coefficients easily comparable across different nodes, we normalize them across all choices of j using the softmax function:

$$\alpha_{ij} = \text{softmax}_j(e_{ij}) = \frac{\exp(e_{ij})}{\sum_{k \in N_i} \exp(e_{ik})} \quad (3)$$

In our experiments, the attention mechanism a is a single-layer feedforward neural network, parametrized by a weight vector $\vec{a} \in \mathbb{R}^{2F'}$, and applying the LeakyReLU nonlinearity. Fully expands out, the coefficients computed by the attention mechanism may then be expressed as:

$$\alpha_{ij} = \frac{\exp\left(\text{LeakyReLU}\left(\vec{a}^T \left[\mathbf{W}\vec{x}_i \parallel \mathbf{W}\vec{x}_j \right]\right)\right)}{\sum_{k \in N_i} \exp\left(\text{LeakyReLU}\left(\vec{a}^T \left[\mathbf{W}\vec{x}_i \parallel \mathbf{W}\vec{x}_k \right]\right)\right)} \quad (4)$$

Where $\|\cdot\|^T$ represents transposition and \parallel is the concatenation operation.

Once obtained, the normalized attention coefficients are used to compute a linear combination of the features corresponding to them, to serve as the final output features for every node.

$$\vec{x}_i = \sigma\left(\sum_{j \in N_i} \alpha_{ij} \mathbf{W}\vec{x}_j\right) \quad (5)$$

σ is an activation function.

2.2 Manifold embedding

Unlike the conventional autoencoder, The proposed model adds a constant-curvature manifold [37][38][39] embedding layer to realize the mapping of the encoder output X' to the constant-curvature Riemann manifold M_k [16][40]. The architecture of the constant-curvature Riemann manifold following the work of Grattarola et al[16]. In the experiments, three manifolds, hyperspherical ($k > 0$), flat ($k = 0$) and hyperbolic ($k < 0$), with $k \in \mathbb{R}$ denoting curvature, are considered and the three mapping encodings are concatenated to form the final encoding.

The special case of null curvature corresponds to the usual Euclidean space. For $k \neq 0$, the d -dimensional manifold M_k can be represented using a $(d+1)$ -dimensional real coordinate system, called the ambient space, and identified by the set of points

$$\{x \in \mathbb{R}^{d+1} \mid \langle x, x \rangle_k = k^{-1}\} \quad (6)$$

Where $\langle \cdot, \cdot \rangle_k$ is a scalar product that depends on the sign of k .

For positive curvature, $\langle x, y \rangle_k = x^T y$ is the usual Euclidean inner product, whereas for a negative curvature

$$\langle x, y \rangle_k = x^T \begin{pmatrix} I_{d \times d} & \mathbf{0} \\ \mathbf{0} & -1 \end{pmatrix} y \quad (7)$$

2.3 Mask-SOM

The last part is the Mask-SOM layer we propose, which implements the manifold feature clustering, and the structure is shown in Figure 1.c. In the past manifold clustering methods, geodesic distance is usually used to measure the correlation between samples. PCA[25][41][42] based on the nearest reconfigurability and maximum separability, the projection transformation of the decentered data samples is used to obtain a new coordinate system, and the projection variance of the sample points under the new coordinate system is maximized. However, the PCA principle is mainly to eliminate the linear correlation between variables and is not applicable to nonlinear dependencies. Mask-SOM is based on the idea of PCA, which selects the direction of maximum variance one by one, but can handle nonlinear dependencies. When measuring vector similarity, it improves the problem of high global similarity caused by small variance features in the input vectors. Mask-SOM achieves the learning of data distribution incrementally by discarding some features randomly in each round of iteration and learning granularity from coarse to fine, and then completes the clustering work. It is worth noting that the dropout value gradually decreases as the training progresses. At the later stage of training, the model gradually stabilizes and the manifold space in which the same class of data exists is homogeneous with the Euclidean space, and the Euclidean distance measure of similarity can be used.

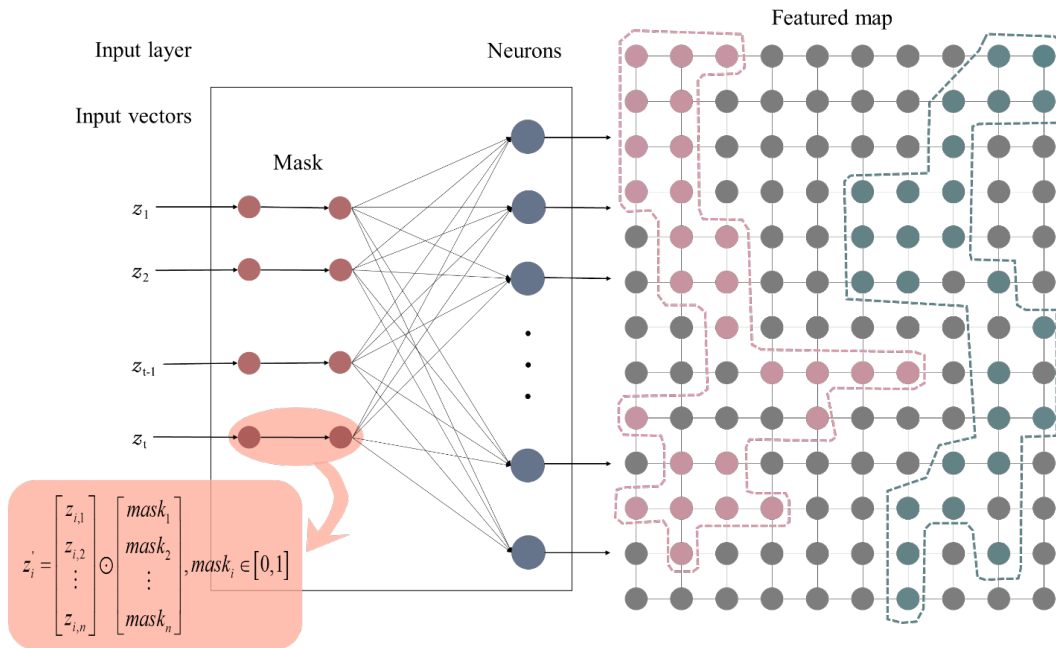


Figure 2 Mask-SOM structure

The learning process of Mask-SOM is as follows:

- 1) Random initialization of the weight vector W_i

2) At time t , the *Mask* matrix is randomly generated based on the dropout values, $Mask \in [0,1]^n$, n denotes the dimensionality of the input vector. Where, $d(t)$ determines the proportion of 0 elements in the *Mask* matrix

3) Sequentially select the input samples z_i , compute the Hadamard product z'_i with the *Mask* matrix, and find the best matching weight vector $w_i(t)$, such that $i^*(t)$ is the winning neuron, then:

$$z'_i = \begin{bmatrix} z_{i,1} \\ z_{i,2} \\ \vdots \\ z_{i,n} \end{bmatrix} \odot \begin{bmatrix} mask_1 \\ mask_2 \\ \vdots \\ mask_n \end{bmatrix}, mask_i \in [0,1] \quad (8)$$

$$i^*(t) = \arg \min \| d(z'_i(t), Mask \odot w_i(t)) \| \quad (9)$$

$$d(z'_i(t), w_i(t)) = \sqrt{(z'_i(t) - Mask \odot w_i(t))^T (z'_i(t) - Mask \odot w_i(t))} \quad (10)$$

4) Update the weights of the winning neuron and its neighbors:

$$w_i(t+1) = w_i(t) + h_{c(x)i} [z_i(t) - w_i(t)] \quad (11)$$

Where, $w_i(t+1)$ is the updated weight of $w_i(t)$, $h_{c(x)i}$ is the neighborhood function, $c(x)$ can be Gaussian Function, Mexican Hat Function or Bubble Function, $h_{c(x)i}$ is calculated by the formula:

$$h_{c(x)i} = \alpha(t) \exp\left(-\frac{\|r_i - r_{c(x)}\|^2}{2\sigma^2(t)}\right) \quad (12)$$

where $\sigma(t)$ denotes the neighborhood radius at moment t , $\alpha(t)$ denotes the learning rate at moment t , $0 < \alpha(t) < 1$, r_i denotes the coordinates of the winner, and $r_{c(x)}$ denotes the coordinates of the collaborator.

5) Update the neighborhood radius $\sigma(t)$, learning rate $\alpha(t)$ and discard rate $d(t)$ by:

$$\alpha(t) = \alpha_0 \left(1 - \frac{t}{T}\right) \quad (13)$$

$$\sigma(t) = \sigma_0 \left(1 - \frac{t}{T}\right) \quad (14)$$

$$d(t) = d_0 \left(1 - \frac{t}{T}\right) \quad (15)$$

6) Repeat steps 2 to 5 until the end of the number of iterations.

3. Intelligent trading system

The opening period of each trading day in the financial market is the most intense period of gaming between traders, featuring high volatility and intensive trading, which is often indicative of the day's trading behavior. Therefore, based on the proposed multidimensional time series clustering model, we build an intelligent quantitative trading system to study and analyze the multidimensional time series formed by specific sectors in the opening session, to predict and trade the sector market of the day.

The opening period in the experiment is the first 30 minutes after the opening of the market. The features are extracted according to the way in Figure 1.a. Sliding window 2 extracts the volatility features of price and sliding window 3 extracts the volatility features of volume, and the sliding window size and sliding step Δt are taken as 10 minutes. After the opening period, the extraction of feature \mathbf{X} for the entire segment is completed, and the extraction formulas are as follows 3-1 and 3-2.

$$P_r = \frac{ClosePrice_{t_0+\Delta t}}{OpenPrice_{t_0}} \quad (16)$$

$$V_r = \frac{\sum_{t=t_0}^{t_0+\Delta t} Volume_T}{\sum_{t=t_0}^{t_0+\Delta t} Volume_Y} \quad (17)$$

where t_0 means the starting time in the sliding window, $Volume_T$ means the volume of the day, and $Volume_Y$ means the volume of the previous day. In the experiment, the financial products in the same segment have pairwise correlation, which means the adjacency matrix A is an all-1 matrix.

The trained Mask-SOM can get a two-dimensional mapping of the data. Based on the real fluctuations of the historical data, the mapping can be divided into three categories and a trading strategy can be developed based on this, as shown in Figure 3. Red represents the future financial sector will have a significant rise, gray represents the future sector fluctuation stable, green represents the future sector will fall. During the testing phase, each new input is mapped to a category so that the corresponding trading strategy is executed: 1): when the test data is classified in the red category, long one of the most active futures in the segment at the next moment after the opening 30 minutes and close the position at the close of the day. 2): When the test data is classified in the green category, short one of the most active futures in the segment at the next moment after the opening 30 minutes and close the position at the close of the day. 3): If the test data is classified in the gray category, it means that the market is inactive and no trades are made on that day.

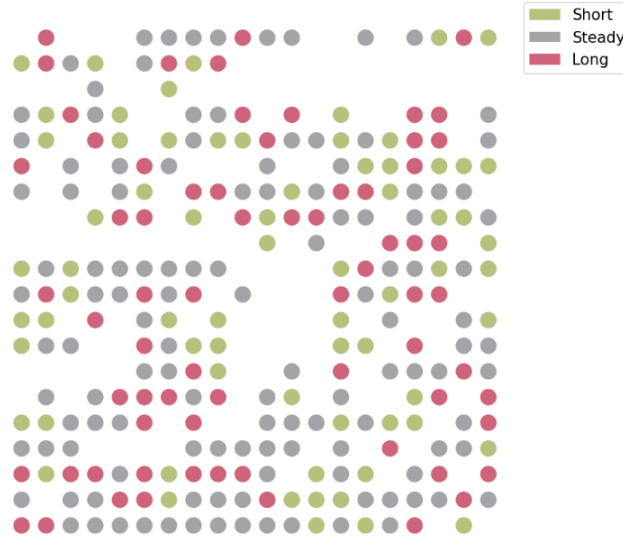


Figure 3 Trading Strategy Examples

3.1 Experiment setups

China commodity futures minute data is used as the experimental dataset, as shown in Table 3-1. Three commodity futures segments, crude oil, non-ferrous metals and ferrous segment, are selected, and the basic information of commodity futures used for trading is listed in the table.

Table 1 Experimental dataset information

Segment	Code	Trading Unit	Tick Size	Margin Rate
Crude Oil Segment	bu	10 ton	RMB 2/ton	15%
	l	5 ton	RMB 5/ton	10%
	pp	5 ton	RMB 1/ton	10%
	TA	5 ton	RMB 2/ton	10%
	v	5 ton	RMB 5/ton	10%
Non-Ferrous Segment	ag	15 kg	RMB 2/kg	10%
	al	5 ton	RMB 5/ton	12%
	au	1000 g	RMB 0.02/g	10%
	cu	5 ton	RMB 10/ton	12%
	ni	1 ton	RMB 10/ton	19%
	pb	5 ton	RMB 5/ton	14%
	sn	1 ton	RMB 10/ton	14%
	zn	5 ton	RMB 5/ton	14%
Ferrous Segment	hc	10 ton	RMB 1/ton	10%
	i	100 ton	RMB 0.5/ton	12%
	j	100 ton	RMB 0.5/ton	15%
	rb	10 ton	RMB 1/ton	10%

To verify the performance of the models, we used three other models for a comparative study.

Model 1) Encoder using GAT, encoding mapping to Euclidean space, using Mask-SOM classification

Model 2) Encoder using GAT, encoding mapping to manifold space, using SOM classification

Model 3) Encoder using GCN, encoding mapping to manifold space, using Mask-SOM classification

Model 4) Our model, encoder using GAT, encodes mapping to the manifold space, using Mask-SOM classification

In addition, the following nine performance indicators will be used to evaluate the performance of the model in the experiments:

- 1) PR: Profit rate
- 2) TN: The total number of trades
- 3) TN+: The number of profitable trades
- 4) TN-: The number of non-profitable trades
- 5) Avg_trade: The average return of all trades:

$$Avg_trade = \frac{PR}{TN}$$

- 6) Avg_profit: The average profits of the profitable trades:

$$Avg_profit = \frac{Total_profits}{TN+}$$

- 7) Avg_loss: The average loss of the non-profitable trades:

$$Avg_loss = \frac{Total_loss}{TN-}$$

- 8) P/L: The profit and loss ratio.
- 9) Accuracy: The decision accuracy.

$$Accuracy = \frac{TN+}{TN}$$

3.2 Crude Oil Segment Experiments

The experiments use historical minute data of the crude oil segment, including the day period (9:00-15:00) and the night period (21:00-early morning of the following day), and the day and night are treated as two separate trading periods in the experiments. All trades are executed in accordance with the aforementioned trading strategy. Set the transaction cost of commodity futures bought in the Crude Oil Segment at 0.2%. The training and test sets were divided by 7:3, and the training set was from 2014.03.03 to 2020.03.18, with 1569 items of data. The test set is from 2020.03.19 to 2021.08.31, with 673 data. Note that instead of setting up a fixed initial capital, we use an upside ratio to measure the effectiveness of the model,

and the single returns discussed in the experiment are the benchmark price spreads of individual commodity futures.

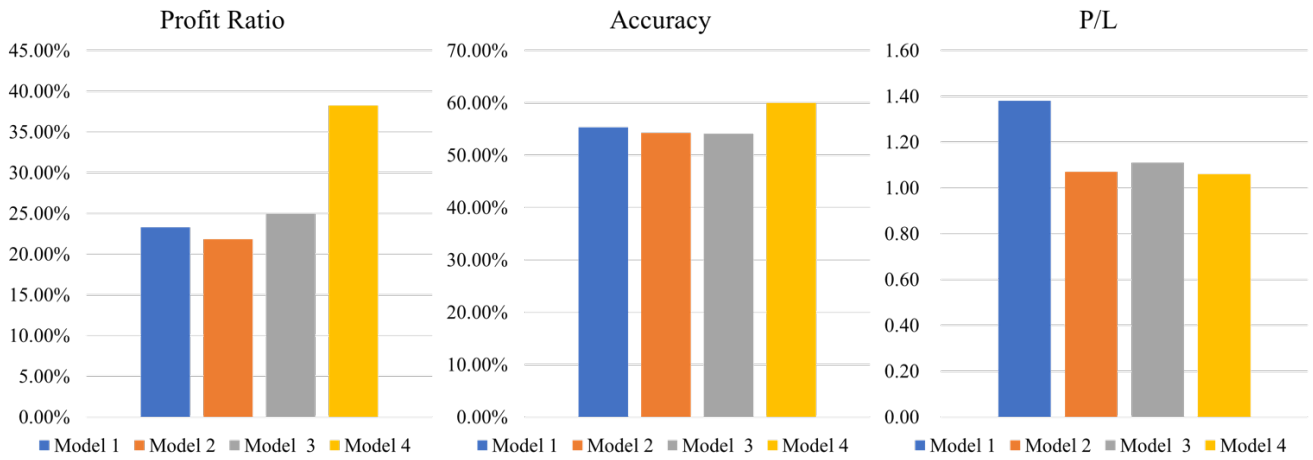


Figure 4 PR, Accuracy and P/L ratio of the four models in the Crude Oil Segment

Figure 4 shows the results of Profit Rate, Accuracy and P/L for the four models in the Crude Oil Segment. As we all know, Accuracy is an important indicator to assess the effectiveness of a forecasting model, and Profit Rate and P/L are important indicators to measure the profitability of a trading system. As can be seen from the figure, our proposed model 4, in terms of profitability and accuracy, far exceeds the other three models, and the profit-loss ratio is also greater than 1, indicating a strong profitability.

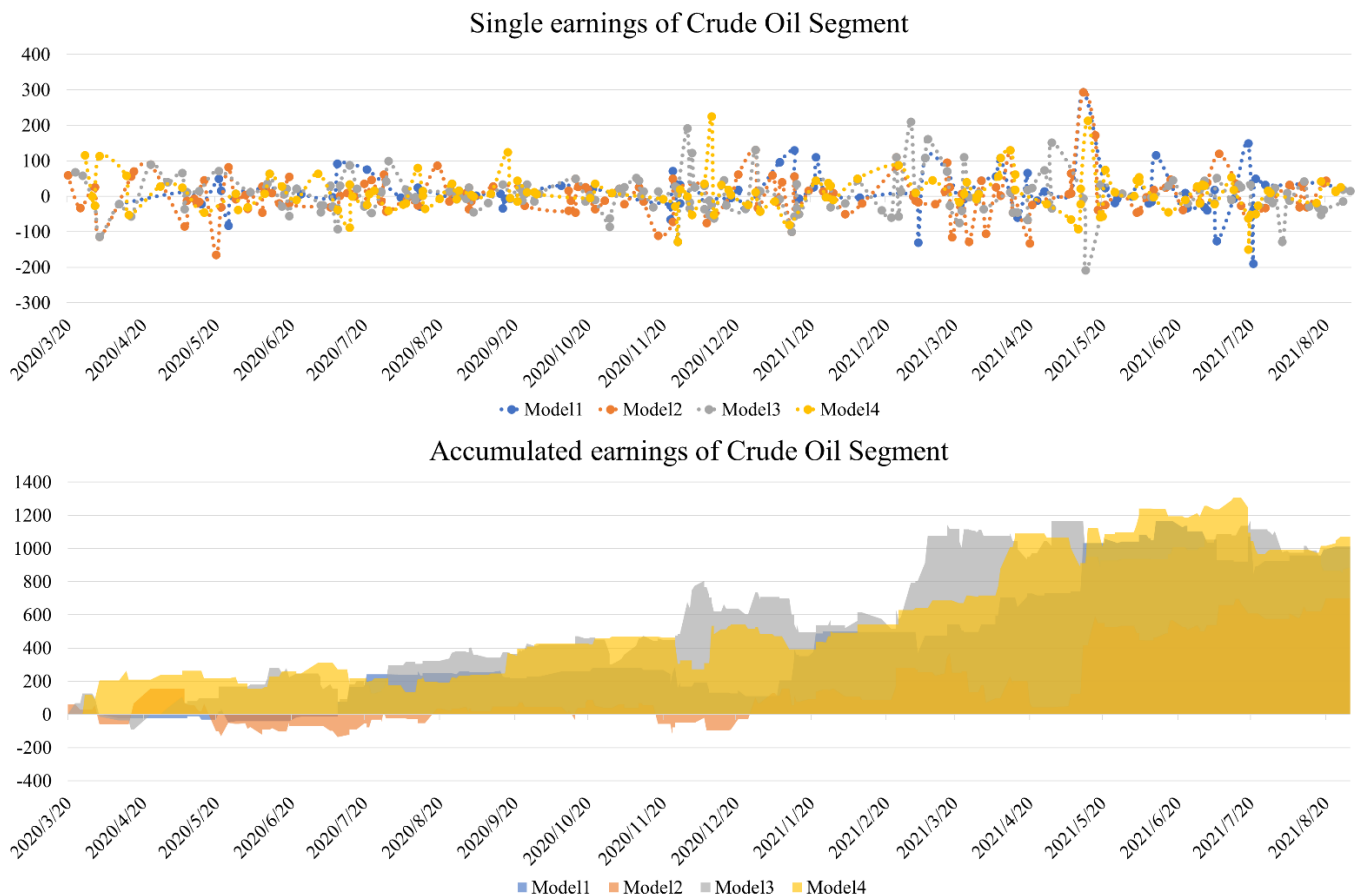


Figure 5 Trading model in the Crude Oil Segment profit chart and cumulative profit area chart

The line chart at the top of Figure 5 shows the profitability of each model for a single trade in the Crude Oil Segment, and when combined with the cumulative profit area chart at the bottom of Figure 5, it can be seen that Model 4 proposed in this paper has a relatively robust overall profit rise compared to the other three models, with higher cumulative profits that can be obtained in a shorter period of time.

The details of this transaction are shown in Table 4-1. From the table, it can be seen that the highest average number of trades is bu (oil bitumen), and models 2, 3 and 4 with manifold encoding have more successful trades for bu (oil bitumen) than model 1, which also shows that analyzing data fluctuations from the perspective of manifold space can effectively avoid the interference of strong nonlinearity. As can be seen in Table 4-2, the proposed model in this paper has the highest profit rate of 38.25% among the 4 models for the period from 2020.03.19 to 2021.08.31, and can obtain the highest accuracy rate of 60.00%. This indicates that the use of GAT to unsupervised learn the relationships among multidimensional time series, and then with Mask-SOM clustering and analysis of manifold space features, can effectively extract and classify the fluctuation types of multidimensional financial time series.

Table 2 Trading details of the test experiments for each model in the crude oil segment

F_Code	LongSuc	LongFail	ShortSuc	ShortFail	F_Code	LongSuc	LongFail	ShortSuc	ShortFail
Strategy 1					Strategy 2				
bu	8	7	17	11	bu	21	21	21	14
l	3	3	3	2	l	4	7	5	5
pp	4	3	2	2	pp	5	2	4	3
TA	5	5	10	9	TA	12	8	5	5
V	0	0	0	0	V	0	0	0	0
Strategy 3					Strategy 4				
bu	20	14	29	19	bu	16	9	27	13
l	5	9	9	6	l	3	1	6	4
pp	5	0	3	4	pp	1	3	4	5
TA	7	14	14	12	TA	3	3	13	10
V	0	0	0	0	V	0	0	0	0

Note: The table headers are the number of successes (LongSuc) and failures (LongFail) for going long, and the number of successes (ShortSuc) and failures (ShortFail) for going short.

Table 3 Experimental results of testing each model in crude oil slab

	PR	TN	TN+	TN-	Avg trade	Avg profit	Avg loss	P/L	Accuracy
Strategy 1	23.28%	94	52	42	10.76	46.90	34.0	1.38	55.32%
Strategy 2	21.80%	142	77	65	4.94	42.75	39.86	1.07	54.23%
Strategy 3	24.93%	170	92	78	5.22	40.54	36.45	1.11	54.12%
Strategy 4	38.25%	121	73	48	8.86	38.53	36.27	1.06	60.00%

The trading strategies of the 4 models in the crude oil segment are given in Figures 6, and the above test experiments were traded according to the corresponding trading strategies.

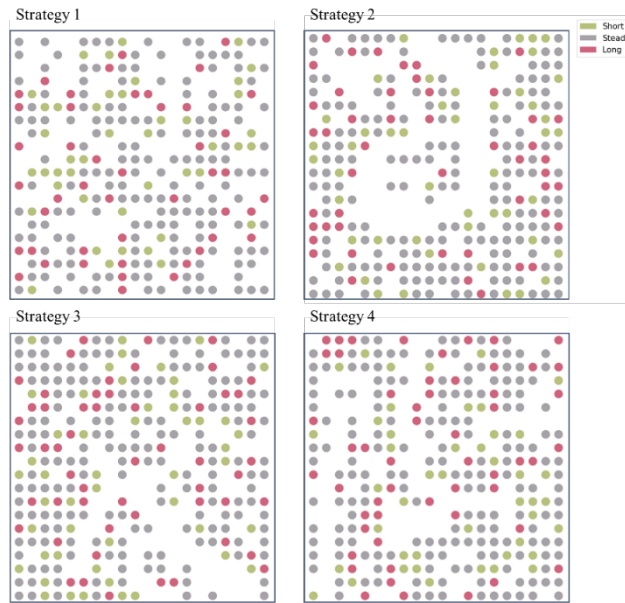


Figure 6 Details of the trading strategies of each model in the Crude Oil Segment

3.3 Non-Ferrous Segment Experiments

In this section, historical minute data of the non-ferrous metals segment is used for the experiment, the trading strategy is maintained, and the trading cost is set the same as that of the crude oil futures segment. The training and test sets are divided according to 7:3, with the training set from 2015.03.27 to 2019.09.05, totaling 2071 items of data, and the test set from 2019.09.06 to 2021.08.31, totaling 888 items of data.

The bar charts in Figures 7 show the results of Profit Rate, Accuracy and P/L for the 4 models in the Non-Ferrous Segment. The graph still shows that model 4 gets the highest Profit Rate. In terms of Accuracy, all 4 trading models have relatively similar accuracy and P/L greater than or equal to 1. It is worth noting that Model 4 has a P/L as high as 1.97, which represents the model's higher profitable ability.

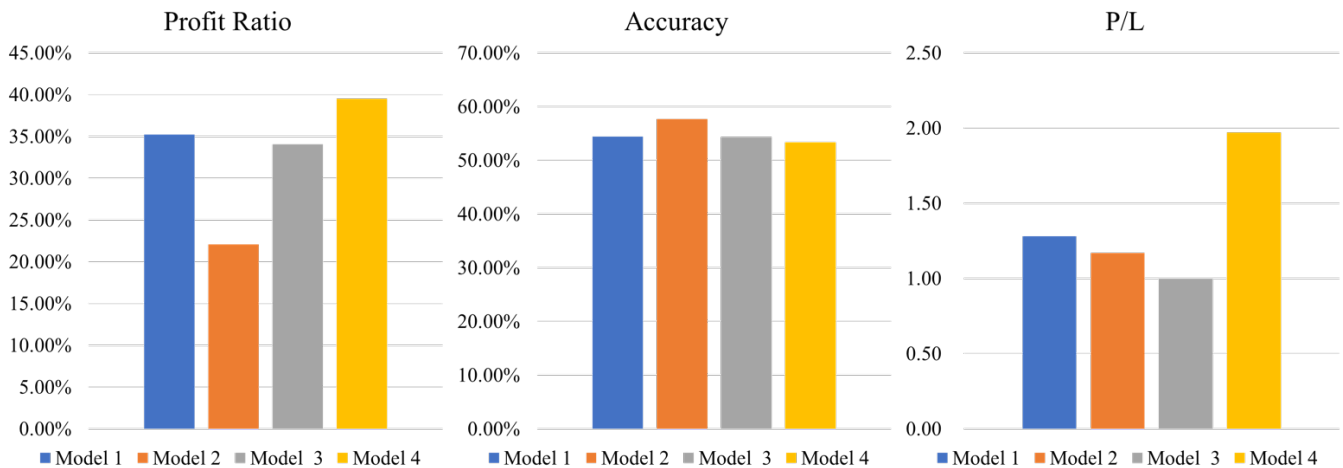


Figure 7 PR, Accuracy and P/L ratio of the four models in the Non-Ferrous Segment

The line graph at the top of Figure 8 represents the profit detail chart of the four models in the nonferrous metals segment, and the area chart at the bottom represents the profit accumulation chart of the four models in the nonferrous metals segment. From the profit accumulation chart, the returns of all four models are relatively robust, but combined with the single profit detail chart, it can be found that the model 4 proposed in this paper has a greater advantage than the other three models in the face of large fluctuations in the financial market.

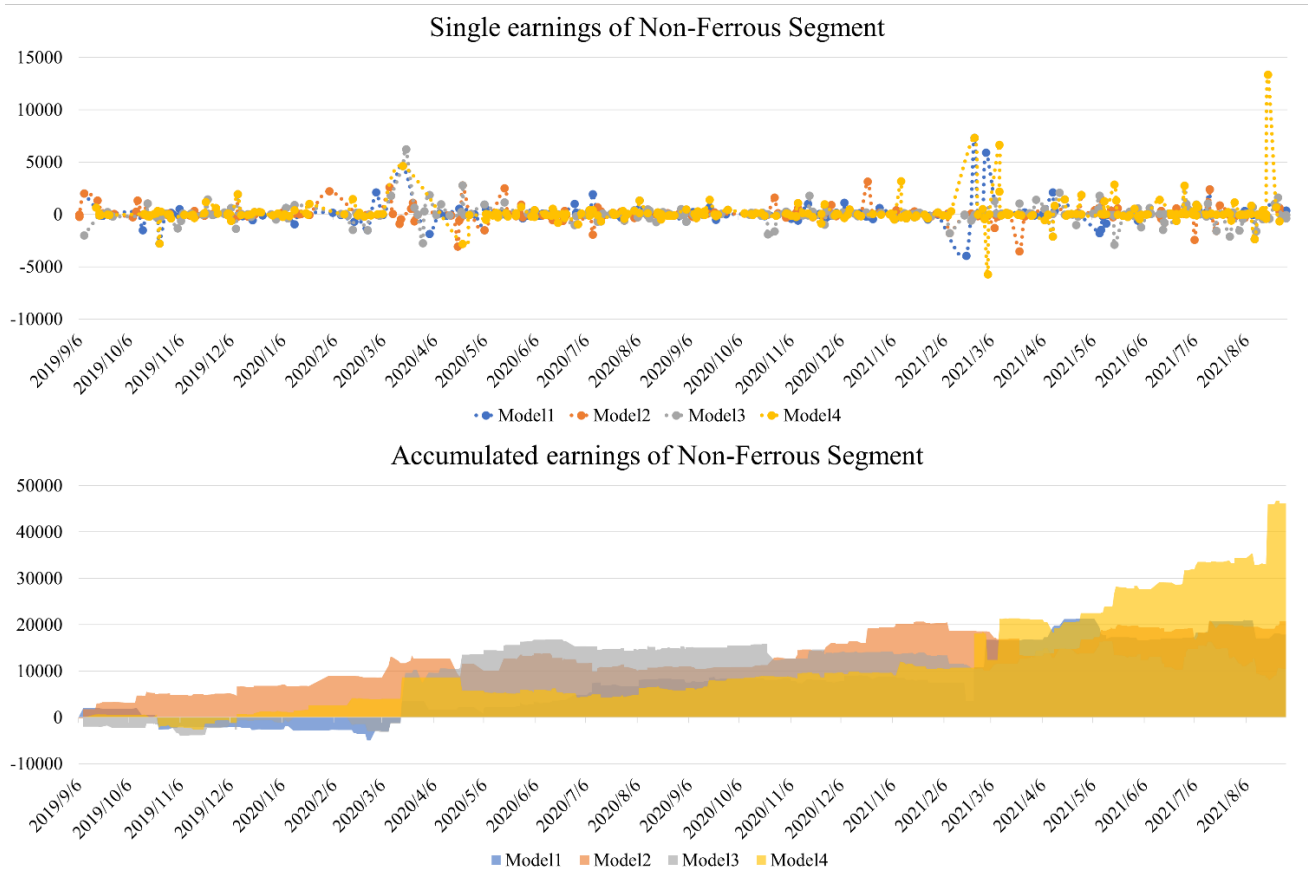


Figure 8 Trading model in Non-Ferrous Segment profit chart and cumulative profit area chart

As can be seen from Table 4, the 4 models have relatively similar trading concerns during this time period. However, when combined with the evaluation indicators in Table 5, Model 4 trades with the smallest average loss, even about 15% lower than Model 2, which is the second lowest loss, and Model 4 trades with the largest average profit, which is about 15% higher than Model 1, which is the second highest average profit, and Model 4 also has the largest average return value, which is about 84% higher than Model 1, which is the second highest average return, and 4.7 times higher than Model 3. This shows the effectiveness of our proposed Model 4 in conducting trades and verifies the accuracy of the P/L.

Table 4 Trading details of the test experiments for each model in the Non-Ferrous Segment

F Code	LongSuc	LongFail	ShortSuc	ShortFail	F Code	LongSuc	LongFail	ShortSuc	ShortFail
--------	---------	----------	----------	-----------	--------	---------	----------	----------	-----------

Strategy 1					Strategy 2				
ag	15	8	6	7	ag	15	13	12	11
al	2	1	1	0	al	1	1	2	2
au	0	0	0	0	au	0	0	0	0
cu	7	7	8	7	cu	11	11	11	7
ni	4	3	4	4	ni	10	5	5	3
pb	12	10	17	11	pb	15	16	11	8
sn	7	4	1	6	sn	8	4	4	2
zn	10	10	11	10	zn	18	10	13	7
Strategy 3					Strategy 4				
ag	16	13	15	17	ag	23	17	18	14
al	2	1	2	0	al	1	2	1	0
au	0	0	0	0	au	0	0	0	0
cu	14	14	8	11	cu	14	15	14	8
ni	8	8	8	7	ni	3	4	5	2
pb	23	10	18	13	pb	17	14	11	13
sn	10	9	0	4	sn	11	3	4	4
zn	15	14	11	5	zn	9	13	11	15

Note: The table headers are the number of successes (LongSuc) and failures (LongFail) for going long, and the number of successes (ShortSuc) and failures (ShortFail) for going short.

Table 5 Experimental results of testing each model in crude oil slab

	PR	TN	TN+	TN-	Avg trade	Avg profit	Avg loss	P/L	Accuracy
Strategy 1	35.23%	193	105	88	94.25	504.76	395.57	1.28	54.40%
Strategy 2	22.05%	236	136	100	87.73	409.4	349.74	1.17	57.63%
Strategy 3	34.04%	276	150	276	36.72	422.56	422.62	1	54.35%
Strategy 4	39.52%	266	142	124	173.29	583.43	296.38	1.97	53.38%

The trading strategies of the 4 models in the Non-Ferrous Segment are given in Figures 9, and the above test experiments were traded according to the corresponding trading strategies.



Figure 9 Details of the trading strategies of each model in the Non-Ferrous Segment

3.4 Ferrous Segment Experiments

In this section, historical minute data of the Ferrous Segment is used for the experiment, and the trading strategy and trading cost are set up in the same way as the other two segments of the experiment. The training and test sets are divided according to 7:3, with the training set from 2014.03.24 to 2019.04.04, with 2323 data, and the test set from 2019.04.04 to 2021.08.31, with 996 data.

The bar chart in Figure 10 shows the Profit Rate, Accuracy and P/L results for the four models in the Ferrous Segment. As can be seen from the chart, model 4 leads by a large margin in terms of Profit Rate, with a Profit Rate twice as high as the other three models. In terms of accuracy, the four trading models have similar accuracy rates, with Model 4 coming in first by a slight margin. In terms of the profit/loss ratio, only model 2 has a lower profit/loss ratio, while the other three models are all greater than 1.

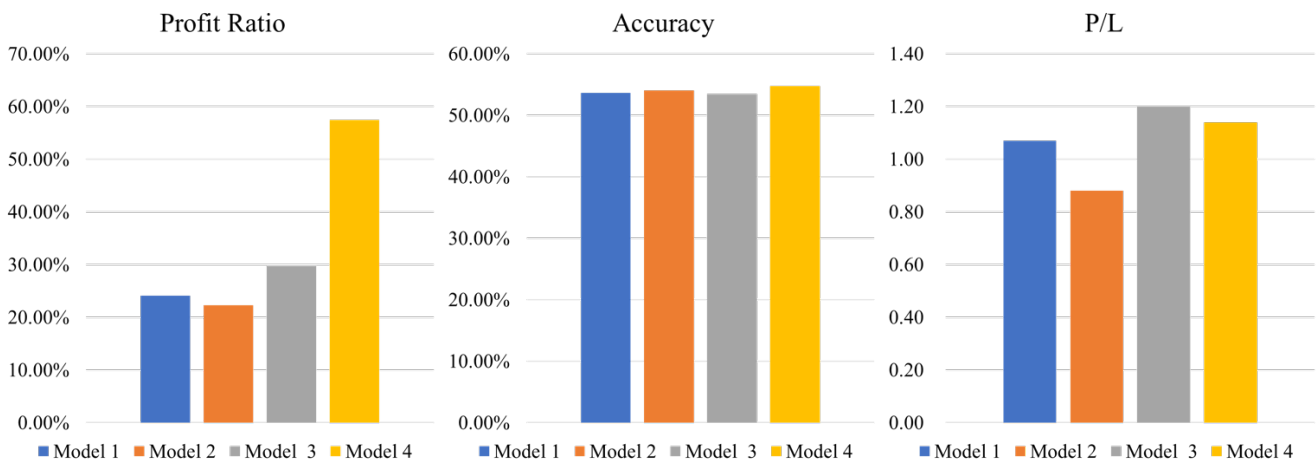


Figure 10 PR, Accuracy and P/L ratio of the four models in the Non-Ferrous Segment

From the cumulative profit area chart at the bottom of Figure 11, we can see that in the early part of the test period, model 4 can maintain profit under the poor performance of models 1, 2 and 3; in the middle of the test period, model 4 misses some trading opportunities and the cumulative profit decreases; in the later part of the test period, there is a significant increase in model 4's gain and the final profit is higher. Combined with the single profit line chart above, we can see that the overall black sector was less volatile in the early period and the investment returns for all four models were relatively small until some large investment opportunities emerged in the later period. In the capture of these opportunities, model 4 was relatively accurate in its judgment, so it ended up with the highest returns.

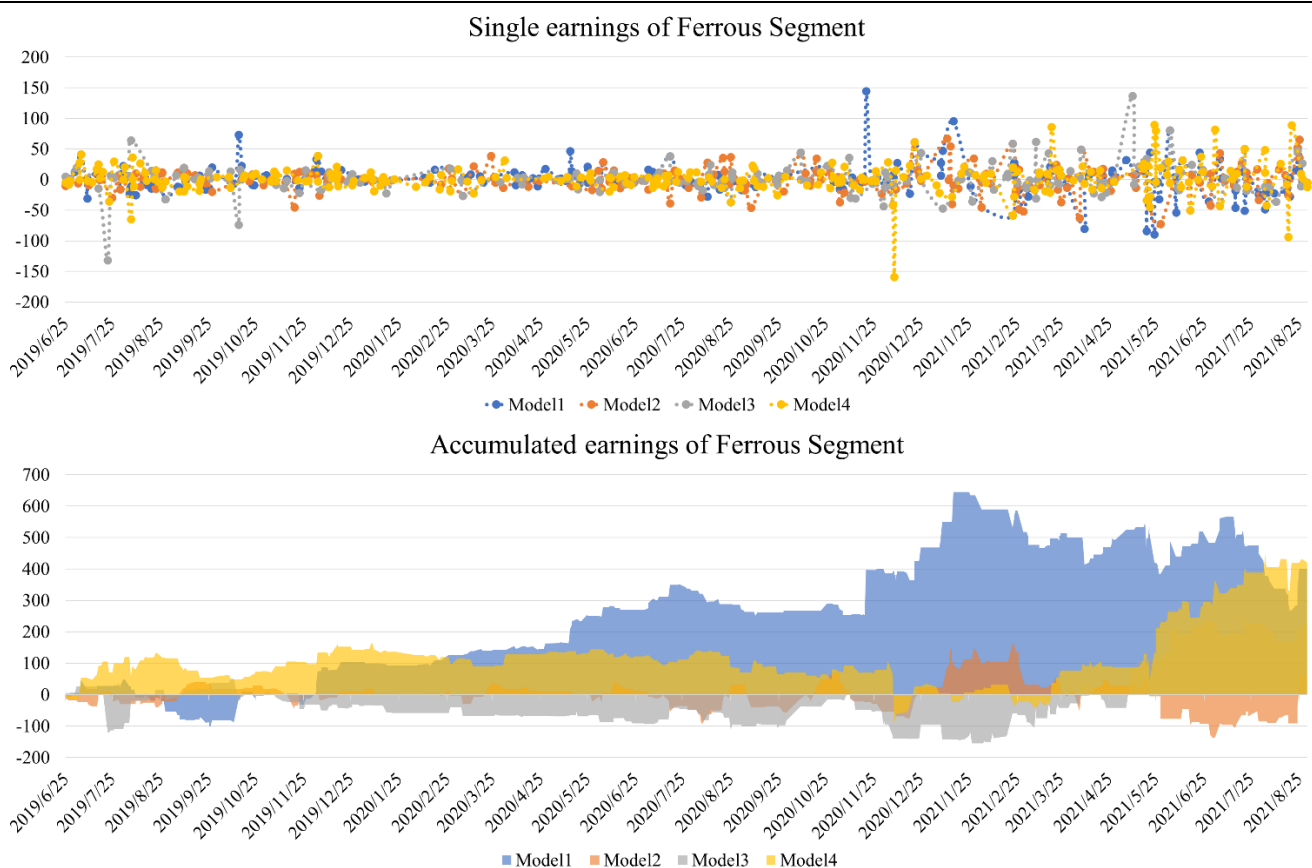


Figure 11 Trading model in Non-Ferrous Segment profit chart and cumulative profit area chart

The details of the test experiments are shown in Tables 6 and 7. As can be seen from Table 6, all four models focus their trading on two commodity futures, i and j. Among them, models 2, 3 and 4 using manifold features analysis capture more trading opportunities on hc futures than model 1 using Euclidean space. From Tables 7, it can be observed that model 4 achieves a return of 57.46%, which is more than twice that of models 1 and 2. In terms of the number of trades, the experimental performance of the four models is similar.

Table 6 Trading details of the test experiments for each model in the Non-Ferrous Segment

F Code	LongSuc	LongFail	ShortSuc	ShortFail	F Code	LongSuc	LongFail	ShortSuc	ShortFail
Strategy 1					Strategy 2				
hc	0	0	1	0	hc	1	3	1	3
i	54	32	32	43	i	48	30	38	29
j	22	15	9	12	j	16	19	16	18
rb	0	0	0	0	rb	0	0	0	0
Strategy 3					Strategy 4				
hc	5	2	1	3	hc	2	2	0	2
i	56	42	20	29	i	59	39	42	35
j	31	14	11	18	j	21	21	8	10
rb	0	0	0	0	rb	0	0	0	0

Note: The table headers are the number of successes (LongSuc) and failures (LongFail) for going long, and the number of successes (ShortSuc) and failures (ShortFail) for going short.

Table 7 Experimental results of testing each model in crude oil slab

	PR	TN	TN+	TN-	Avg trade	Avg profit	Avg loss	P/L	Accuracy
Strategy 1	24.12%	220	118	102	1.8	17.17	15.99	1.07	53.63%
Strategy 2	22.32%	222	120	222	0.28	13.77	15.59	0.88	54.05%
Strategy 3	29.75%	232	124	108	2.35	16.15	13.49	1.2	53.45%
Strategy 4	57.46%	241	132	109	1.72	14.9	14.23	1.14	54.78%

The trading strategies of the 4 models in the Non-Ferrous Segment are given in Figures 9, and the above test experiments were traded according to the corresponding trading strategies.

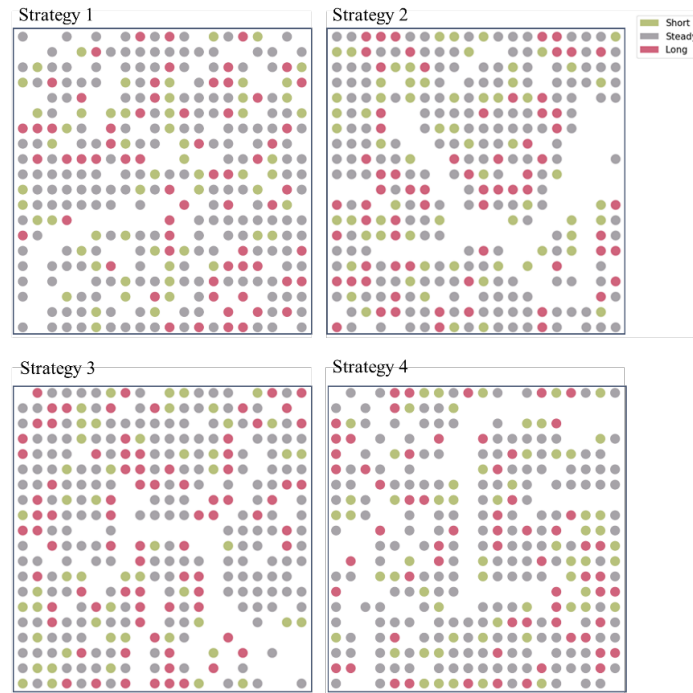


Figure 12 Details of the trading strategies of each model in the Crude Oil Segment

4. Conclusions

In this paper, we propose a novel manifold clustering model based on graph attention autoencoder and construct a quantitative trading system for commodity futures based on it. To cope with the strong nonlinearity of multidimensional time series, we introduce constant curvature Riemannian manifolds into the graph attention network and realize the transfer of fluctuation features from Euclidean space to the manifold space analysis. To solve the timeliness problem of streaming space feature clustering, we propose Mask-SOM, which adopts a recursive clustering approach from coarse to detailed to realize the clustering analysis of financial time series streaming features. Comparative test experiments are conducted using data from multiple commodity futures segments, based on nine evaluation indexes such as profitability and accuracy, to validate against the utility and effectiveness of the model.

References

- [1] Kohonen T. The self-organizing map[J]. *Proceedings of the IEEE*, 1990, 78(9): 1464-1480.
- [2] Hsu S H, Hsieh J J P A, Chih T C, et al. A two-stage architecture for stock price forecasting by integrating self-organizing map and support vector regression[J]. *Expert Systems with Applications*, 2009, 36(4): 7947-7951.
- [3] Sarlin P, Eklund T. Fuzzy clustering of the self-organizing map: some applications on financial time series[C]//*International Workshop on Self-Organizing Maps*. Springer, Berlin, Heidelberg, 2011: 40-50.
- [4] Tay F E H, Cao L J. Improved financial time series forecasting by combining support vector machines with self-organizing feature map[J]. *Intelligent Data Analysis*, 2001, 5(4): 339-354.
- [5] Afolabi M O, Olude O. Predicting stock prices using a hybrid Kohonen self organizing map (SOM)[C]//*2007 40th Annual Hawaii International Conference on System Sciences (HICSS'07)*. IEEE, 2007: 48-48.
- [6] Eklund T, Back B, Vanharanta H, et al. Using the self-organizing map as a visualization tool in financial benchmarking[J]. *Information Visualization*, 2003, 2(3): 171-181.
- [7] Fu T, Chung F, Ng V, et al. Pattern discovery from stock time series using self-organizing maps[C]//*Workshop Notes of KDD2001 Workshop on Temporal Data Mining*. New York, NY, USA: Springer, 2001, 1.
- [8] Velickovic P, Cucurull G, Casanova A, et al. Graph attention networks[J]. *stat*, 2017, 1050: 20.
- [9] Zhao H, Wang Y, Duan J, et al. Multivariate time-series anomaly detection via graph attention network[C]//*2020 IEEE International Conference on Data Mining (ICDM)*. IEEE, 2020: 841-850.
- [10] Cheng R, Li Q. Modeling the Momentum Spillover Effect for Stock Prediction via Attribute-Driven Graph Attention Networks[C]//*Proceedings of the AAAI Conference on Artificial Intelligence*. 2021, 35(1): 55-62.
- [11] Kipf T N, Welling M. Semi-supervised classification with graph convolutional networks[J]. *arXiv preprint arXiv:1609.02907*, 2016.
- [12] Badrinarayanan V, Kendall A, Cipolla R. Segnet: A deep convolutional encoder-decoder architecture for image segmentation[J]. *IEEE transactions on pattern analysis and machine intelligence*, 2017, 39(12): 2481-2495.
- [13] Kingma D P, Welling M. Auto-encoding variational bayes[J]. *arXiv preprint arXiv:1312.6114*, 2013.
- [14] Salehi A, Davulcu H. Graph attention auto-encoders[J]. *arXiv preprint arXiv:1905.10715*, 2019.
- [15] Kosaraju V, Sadeghian A, Martín-Martín R, et al. Social-bigat: Multimodal trajectory forecasting using bicycle-gan and graph attention networks[J]. *Advances in Neural Information Processing Systems*, 2019, 32.
- [16] Grattarola D, Zambon D, Livi L, et al. Change detection in graph streams by learning graph embeddings on constant-

curvature manifolds[J]. IEEE Transactions on neural networks and learning systems, 2019, 31(6): 1856-1869.

[17] Vlachos M, Lin J, Keogh E, et al. A wavelet-based anytime algorithm for k-means clustering of time series[C]//In proc. workshop on clustering high dimensionality data and its applications. 2003.

[18] Guo C, Jia H, Zhang N. Time series clustering based on ICA for stock data analysis[C]//2008 4th international conference on wireless communications, networking and mobile computing. IEEE, 2008: 1-4.

[19] Huang X, Ye Y, Xiong L, et al. Time series k-means: A new k-means type smooth subspace clustering for time series data[J]. Information Sciences, 2016, 367: 1-13.

[20] Hsu Y C, Chen A P. A clustering time series model for the optimal hedge ratio decision making[J]. Neurocomputing, 2014, 138: 358-370.

[21] Ultsch A. Data mining and knowledge discovery with emergent self-organizing feature maps for multivariate time series[M]//Kohonen maps. Elsevier science BV, 1999: 33-45.

[22] Aghabozorgi S, Shirkhorshidi A S, Wah T Y. Time-series clustering—a decade review[J]. Information Systems, 2015, 53: 16-38.

[23] Niennattrakul V, Ratanamahatana C A. On clustering multimedia time series data using k-means and dynamic time warping[C]//2007 International Conference on Multimedia and Ubiquitous Engineering (MUE'07). IEEE, 2007: 733-738.

[24] Liu J, Bai Y, Kang J, et al. A new approach to hierarchical clustering using partial least squares[C]//2006 International Conference on Machine Learning and Cybernetics. IEEE, 2006: 1125-1131.

[25] Zhou Z H. Ensemble learning[M]//Machine learning. Springer, Singapore, 2021: 181-210.

[26] Tenenbaum J B, Silva V, Langford J C. A global geometric framework for nonlinear dimensionality reduction[J]. science, 2000, 290(5500): 2319-2323.

[27] Balasubramanian M, Schwartz E L. The isomap algorithm and topological stability[J]. Science, 2002, 295(5552): 7-7.

[28] Mordohai P, Medioni G G. Unsupervised Dimensionality Estimation and Manifold Learning in high-dimensional Spaces by Tensor Voting[C]//IJCAI. 2005: 798-803.

[29] Goh A, Vidal R. Segmenting motions of different types by unsupervised manifold clustering[C]//2007 IEEE Conference on Computer Vision and Pattern Recognition. IEEE, 2007: 1-6.

[30] Wang Y, Jiang Y, Wu Y, et al. Spectral clustering on multiple manifolds[J]. IEEE Transactions on Neural Networks, 2011, 22(7): 1149-1161.

[31] Nie F, Xu D, Tsang I W H, et al. Flexible manifold embedding: A framework for semi-supervised and unsupervised dimension reduction[J]. IEEE Transactions on Image Processing, 2010, 19(7): 1921-1932.

-
- [32] Elhamifar E, Vidal R. Sparse manifold clustering and embedding[J]. Advances in neural information processing systems, 2011, 24.
- [33] Roweis S T, Saul L K. Nonlinear dimensionality reduction by locally linear embedding[J]. science, 2000, 290(5500): 2323-2326.
- [34] Han M, Feng S, Chen C L P, et al. Structured manifold broad learning system: A manifold perspective for large-scale chaotic time series analysis and prediction[J]. IEEE Transactions on Knowledge and Data Engineering, 2018, 31(9): 1809-1821.
- [35] Feng S, Ren W, Han M, et al. Robust manifold broad learning system for large-scale noisy chaotic time series prediction: A perturbation perspective[J]. Neural Networks, 2019, 117: 179-190.
- [36] Papaioannou P, Talmon R, di Serafino D, et al. Time Series Forecasting Using Manifold Learning[J]. arXiv preprint arXiv:2110.03625, 2021.
- [37] Wilson R C, Hancock E R, Pekalska E, et al. Spherical and hyperbolic embeddings of data[J]. IEEE transactions on pattern analysis and machine intelligence, 2014, 36(11): 2255-2269.
- [38] Jain B J. On the geometry of graph spaces[J]. Discrete Applied Mathematics, 2016, 214: 126-144.
- [39] Lin T, Zha H. Riemannian manifold learning[J]. IEEE Transactions on Pattern Analysis and Machine Intelligence, 2008, 30(5): 796-809.
- [40] Zambon D, Livi L, Alippi C. Anomaly and change detection in graph streams through constant-curvature manifold embeddings[C]//2018 International Joint Conference on Neural Networks (IJCNN). IEEE, 2018: 1-7.
- [41] Wold S, Esbensen K, Geladi P. Principal component analysis[J]. Chemometrics and intelligent laboratory systems, 1987, 2(1-3): 37-52.
- [42] Abdi H, Williams L J. Principal component analysis[J]. Wiley interdisciplinary reviews: computational statistics, 2010, 2(4): 433-459.